Inorganic Chemistry

Article

Cite This: Inorg. Chem. XXXX, XXX, XXX-XXX

pubs.acs.org/IC

Hydrogenation Properties of Laves Phases $LnMg_2$ (Ln = La, Ce, Pr, Nd, Sm, Eu, Gd, Tb, Ho, Er, Tm, Yb)

Anton Werwein,[†] Florian Maaß,[†] Leonhard Y. Dorsch,[†] Oliver Janka,[‡] Rainer Pöttgen,[‡] Thomas C. Hansen,[§] Justin Kimpton,[∥] and Holger Kohlmann*,[†]

[†]Department of Inorganic Chemistry, Leipzig University, Johannisallee 29, 04103 Leipzig, Germany

[‡]Institut für Anorganische und Analytische Chemie, Universität Münster, Corrensstrasse 30, 48149 Münster, Germany

[§]Institut Laue-Langevin, 71 Avenue des Martyrs, 38000 Grenoble, France

[∥]Australian Synchrotron, 800 Blackburn Road, Clayton, Melbourne, Australia

Supporting Information

ABSTRACT: The hydrogenation properties of Laves phases $LnMg_2$ (Ln = La, Ce, Pr, Nd, Sm, Eu, Gd, Tb, Ho, Er, Tm, Yb) were investigated by thermal analysis, X-ray, synchrotron, and neutron powder diffraction. At 14.0 MPa hydrogen gas pressure and 393 K, $PrMg_2$ and $NdMg_2$ take up hydrogen and form the colorless, ternary hydrides $PrMg_2H_7$ ($P4_12_12$, a = 632.386(6) pm, c = 945.722(11) pm) and $NdMg_2H_7$ ($P4_12_12$, a = 630.354(9) pm, c = 943.018(16) pm). The crystal structures were refined by the Rietveld method from neutron powder diffraction data on the deuterides ($PrMg_2D_7$, $P4_12_12$, a = 630.56(2) pm, c = 943.27(3) pm; $NdMg_2D_7$, $P4_12_12$, a = 628.15(2) pm, c = 940.32(3) pm) and shown to be isotypic to $LaMg_2D_7$. The $LaMg_2D_7$ type of hydrides decompose at 695 K (La), 684 K (Ce), 684 K (Pr), 672 K (Nd), and 639 K (Sm) to lanthanide hydrides and magnesium. The Laves phase $EuMg_2$ forms a hydride $EuMg_2H_x$ of black color. Its crystal structure ($P2_12_12_1$, a = 664.887(4) pm, b = 1136.993(7) pm, c = 1069.887(7) pm) is closely related to the hexagonal Laves phase ($MgZn_2$ type) of the hydrogen-free parent intermetallic. $GdMg_2$ and $TbMg_2$ form hydrides $GdMg_2H_x$ with orthorhombic unit cells (a = 1282.7(4) pm, b = 572.5(2) pm, c = 881.7(2) pm) and $TbMg_2H_x$ (a = 617.8(3) pm, b = 1045.8(8) pm, c = 997.1(5) pm), presumably also with a distorted $MgZn_2$ type of structure. $CeMg_2H_7$ and $NdMg_2H_7$ are paramagnetic with effective magnetic moments of 2.49(1) μ_B and 3.62(1) μ_B, respectively, in good agreement with the calculated magnetic moments of the free trivalent rare-earth cations ($\mu_{calc}(Ce^{3+})$ = 2.54 μ_B; $\mu_{calc}(Nd^{3+})$ = 3.62 μ_B).

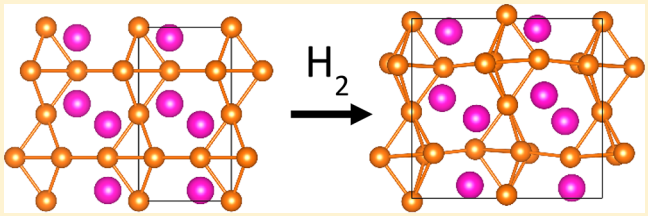

1. INTRODUCTION

Lanthanide containing hydrides are a fascinating class of compounds with a wide range of compositions, crystal structures, and bonding properties, ranging from ionic[1,2] to metallic[3−5] and complex hydrides.[6,7] Laves phases are a large group of intermetallic compounds with the composition AM_2, where A is the larger atom. The three most common structure types are cubic $MgCu_2$ (C15), hexagonal $MgZn_2$ (C14), and $MgNi_2$ (C36). Many Laves phases can be used for hydrogen storage, since they reversibly take up large amounts of hydrogen.[8,9] In the crystal structures of the hydrides, hydrogen atoms often occupy tetrahedral voids surrounded by two atoms each of A and M, [A_2M_2], and tetrahedral voids surrounded by one A and three M atoms, [AM_3].[10−18] In lanthanide-containing Laves phases $LnMg_2$ the lanthanide atoms Ln always occupy the A sites due to their large size.[19] Laves phases $LnMg_2$ of the early lanthanides Ln = La−Gd with the exception of europium crystallize in the cubic $MgCu_2$ (C15) type; those with Ln = Eu and Tb−Lu crystallize in the hexagonal $MgZn_2$ (C14) type of structure (Table 1). $LnMg_2$ (Ln = La, Ce, Sm) were found to absorb large amounts of hydrogen. They form isotypic hydrides $LnMg_2H_7$ with the highest hydrogen content observed for Laves phases so far, while undergoing a metal−semiconductor transition.[20,21] The hydrogen atoms occupy four different crystallographic sites and are coordinated tetrahedrally by two Ln and two Mg atoms, [Ln_2Mg_2], by four Mg atoms, [Mg_4], or by two Ln and one Mg atom in a trigonal-planar fashion, [Ln_2Mg]. The crystal structures ($LaMg_2D_7$ type) show a close relationship to the parent cubic Laves phase, which becomes expanded and distorted upon hydrogen incorporation. Europium is an exception both in the series of Laves phases (Table 1) and in the hydrides. The hexagonal Laves phase $EuMg_2$ forms a hydride $EuMg_2H_6$. This is the only hydride of a Laves phase $LnMg_2$ containing divalent lanthanide ions. Its crystal structure shows no resemblance to any of the Laves phase structure types. It represents a tetragonal defect-variant of the cubic perovskite type,[22,23] which is another common structure type for metal hydrides.[24−26] Despite the favorable environmental properties, the high molar content, and the good volume efficiency for hydrogen,[20] the hydrides $LnMg_2H_7$ known so far are not very promising candidates for hydrogen

Received: September 12, 2017

DOI: 10.1021/acs.inorgchem.7b02319
Inorg. Chem. XXXX, XXX, XXX−XXX

Table 1. Structure Types of Laves Phases $LnMg_2$[a] and Their Hydrides[b]

$LaMg_2$	**$CeMg_2$**	**$PrMg_2$**	**$NdMg_2$**	**$SmMg_2$**	***$EuMg_2$***		**$GdMg_2$**
$LaMg_2H_7$[20]	$CeMg_2H_7$[20]	$PrMg_2H_7$ [this work]	$NdMg_2H_7$ [this work]	$SmMg_2H_7$[21]	$EuMg_2H_6$,[22] $EuMg_2H_x$ [this work]		$GdMg_2H_x$ [this work]
	$TbMg_2$	*$DyMg_2$*	*$HoMg_2$*	*$ErMg_2$*	*$TmMg_2$*	*$YbMg_2$*	*$LuMg_2$*
	$TbMg_2H_x$ [this work]						

[a]First row, Ln = lanthanides, **$MgCu_2$ structure type (C15) in bold**, *$MgZn_2$ structure type in italics*. [b]Second row, $LnMg_2H_7$ in $LaMg_2H_7$ type of structure, $EuMg_2H_6$ own structure type.

storage. They need high hydrogen pressures to form, exhibit only moderate weight efficiencies, and release hydrogen at rather high temperatures and irreversibly. In this work, the hydrogenation behavior of Laves phases $LnMg_2$ of the remaining lanthanides Ln = Pr, Nd, Gd, Tb, Ho, Er, Tm, Yb (Table 1) are investigated, which have not been reported yet to form hydrides. The aim of this study is to rationalize the formation and decomposition conditions of the hydrides, since these properties are crucial for possible hydrogen storage applications.

2. EXPERIMENTAL SECTION

Syntheses. Because of the air sensitivity of the compounds all handlings were performed in an argon-filled glovebox. Lanthanide metals (La, Ce, Nd, Eu: Chempur, Sm: Alfa Aesar, Gd, Tb, Er, Yb: Kristallhandel Kelpin, all with a purity of 99.9% or better) were surface-cleaned, cut into small pieces, and mixed with magnesium powder (abcr, 99.8%) in a stoichiometric 1:2 ratio. These mixtures were sealed in niobium ampules, which were heated under vacuum in a tube furnace to 1173 K and subsequently quenched in water. The products were annealed below the peritectic decomposition temperature of the Laves phases $LnMg_2$.[27] For preparation of the hydrides (deuterides), well-ground samples $LnMg_2$ were placed in crucibles made from hydrogen-resisting Böhler L718-V alloy and reacted with hydrogen (deuterium) gas (hydrogen: Air Liquide, 99.9%; deuterium, Air Liquide, 99.8%) in autoclaves made from the same alloy. The temperature was increased with 10 K/h and kept at the maximum for 48 h (see Table 2 for gas pressures and temperatures). After the annealing time the autoclave was cooled naturally. Replacing 5 mol % of neodymium by samarium or terbium in the synthesis procedure led to substituted samples as described below. The hydrogenation reaction was performed in analogy to $NdMg_2H_7$.

Thermal Analysis. Hydrogenation experiments were performed in a differential scanning calorimeter (DSC) Q1000 from TA Instruments equipped with a gas pressure cell.[28] The powdered samples (10−30 mg) were loaded in aluminum pans, which were subsequently crimped. The experiments were done with a heating rate of 10 K/min under a hydrogen atmosphere of 5.0 MPa at 298 K, which rose to 6.7 MPa at the final temperature of 703 K.

X-ray Powder Diffraction. X-ray powder diffraction data were collected on a Huber G670 camera with image plate system using Mo Kα1 or Cu Kα1 radiation. Flat transmission samples were prepared by grinding the moisture-sensitive powders in an argon atmosphere, mixing with apiezon grease, and putting the sample between two sheets of capton foil.

In Situ X-ray Powder Diffraction. In situ X-ray powder diffraction was performed on a Huber G670 diffractometer with image plate system and Mo Kα1 radiation (10 min data collection time per temperature and 10 K temperature steps). The sample was enclosed in a quartz capillary of 0.3 mm diameter, which was connected to a gas control system.[29]

Synchrotron Powder Diffraction. Synchrotron powder diffraction experiments were performed on samples in sealed glass capillaries of 0.3 mm diameter at the Australian synchrotron powder diffraction beamline with a wavelength λ = 58.9074 pm. Data collection time was 20 min.

Neutron Powder Diffraction. Neutron powder diffraction was performed at the Institut Laue-Langevin in Grenoble, France, at the high-flux diffractometer D20 in high-resolution mode. Powdered samples were placed in indium-sealed vanadium containers with 6 mm inner diameter. Data collection times were 75 min for $NdMg_2D_7$ and 15 min for $PrMg_2D_7$, and the wavelengths were calibrated using silicon (NIST640b) as an external standard.

Table 2. Experimental Conditions and Products of Hydrogenation Experiments[a]

Laves phase	T_{max}, K	$p(H_2)$, MPa	t, h	products
$LaMg_2$	703	5.0	2	*LaH_3, MgH_2*
	393	**14**	**48**	**$LaMg_2H_7$**
$CeMg_2$	703	5	2	*CeH_3, MgH_2*
	393	**14**	**48**	**$CeMg_2H_7$**
$PrMg_2$	**393**	**9.5**	**48**	**$PrMg_2H_7$**
$NdMg_2$	703	5	2	*NdH_2,NdH_{2+x},MgH_2*
	393	**14**	**48**	**$NdMg_2H_7$**
$SmMg_2$	703	5	2	*SmH_2, SmH_{2+x},MgH_2*
	393	**14**	**48**	**$SmMg_2H_7$**
$EuMg_2$	703	5	2	*$EuMg_2H_6$, $EuMgH_4$*
	353	**12**	**48**	**$EuMg_2H_x$**
$GdMg_2$	723	5	2	*GdH_2,GdH_{2+x}*
	473	**14**	**48**	**$GdMg_2H_x$**
$TbMg_2$	723	5	2	*TbH_2,TbH_{2+x},TbH_3, MgH_2*
	473	**14**	**48**	**$TbMg_2H_x$**
$HoMg_2$	703	5	2	*HoH_2,HoH_{2+x}*
	473	**14**	**48**	**HoH_2,HoH_{2+x}**
$ErMg_2$	673	5	2	*ErH_2,ErH_{2+x},ErH_3*
	473	**14**	**48**	*ErH_2,ErH_{2+x}*
$TmMg_2$	723	5	2	*TmH_2,TmH_{2+x}, TmH_3, Mg*
	473	**14**	**48**	**TmH_2**
$YbMg_2$	703	5	2	*YbH_2, $YbH_{2.63}$, $Yb_4Mg_3H_{14}$, $Yb_{19}Mg_8H_{54}$*
	393	**8**	**2**	**$YbMg_2$, $YbH_{2.63}$**

[a]Experiments were in a *differential scanning calorimeter* (*italics*) and **autoclaves** (**bold**).

Rietveld Refinement.[30,31] The crystal structures were refined using the software package TOPAS[32] for X-ray and synchrotron diffraction data and with the FULLPROF software package for neutron diffraction data.[33,34] The crystal structures were visualized with VESTA.[35] Additional crystallographic information is available in the Supporting Information.

Magnetic Measurement. The powdered samples of $CeMg_2H_7$ and $NdMg_2H_7$ were packed into polyethylene (PE) capsules in an argon-filled glovebox and attached to the sample holder rod of a Vibrating Sample Magnetometer unit (VSM) for measuring the magnetization $M(T, H)$ in a Quantum Design Physical Property Measurement System (PPMS). The samples were investigated in the temperature range of 2.5−300 K with magnetic flux densities up to 80 kOe.

3. RESULTS AND DISCUSSION

Hydrogenation Reactions. The synthesis of the Laves phases yielded single-phase products according to X-ray powder diffraction except for $NdMg_2$ and $GdMg_2$, which

DOI: 10.1021/acs.inorgchem.7b02319
Inorg. Chem. XXXX, XXX, XXX−XXX

exhibit up to 20 wt % byproducts (NdMg, GdMg). Lattice parameters refined by the Rietveld method are in good agreement with literature values. All samples take up considerable amounts of hydrogen and form binary or ternary hydrides (Table 2). Low to moderate hydrogen gas pressure and high temperature seem to favor the formation of mixtures of the binary hydrides LnH_{2-3} and MgH_2. These samples appear black after hydrogenation. In some cases no crystalline magnesium species can be identified by X-ray powder diffraction. Exceptions from this finding are $EuMg_2$ and $YbMg_2$. The former yields red $EuMg_2H_6$, while the latter yields a black powder consisting of four different binary and ternary hydrides. Ternary Laves phase hydrides $LnMg_2H_7$ were obtained only at higher hydrogen gas pressures (≥9.5 MPa) and moderate temperatures (393 K). Among them are the new compounds $PrMg_2H_7$ and $NdMg_2H_7$ (crystal structures and chemical and physical properties vide infra). Under similar conditions, $EuMg_2$, $GdMg_2$, and $TbMg_2$ react to new hydrogen-containing phases $LnMg_2H_x$. The ternary Laves phase hydrides $LnMg_2H_7$ are colorless (Ln = Pr, Nd), red (Ln = Ce), and green (Ln = Sm) powders, while $LnMg_2H_x$ (Ln = Eu, Gd, Tb) are black powders. Small impurities of the binary hydrides LnH_{2+x} or LnH_{3-x} may also lead to a black appearance of the samples. The ternary hydrides except for $EuMg_2H_x$ are stable in air. The remaining Laves phases $LnMg_2$ (Ln = Er, Ho, Tm, Yb) react with hydrogen to form binary lanthanide hydrides, of which ErH_2 and HoH_2 show very poor crystallinity, and no trace of any crystalline magnesium-containing compound.

Crystal Structures of $LnMg_2H_7$ (Ln = La, Ce, Pr, Nd, Sm). The X-ray powder diffraction patterns of the two new phases $PrMg_2H_7$ and $NdMg_2H_7$ could be indexed with tetragonal cells similar to those of $CeMg_2H_7$ and $SmMg_2H_7$. This suggests the crystal structure to belong to the $LaMg_2D_7$ type, which is confirmed by the good correspondence of calculated and measured X-ray powder diffraction data ($PrMg_2H_7$, $P4_12_12$, a = 632.386(6) pm, c = 945.722(11) pm; $NdMg_2H_7$, $P4_12_12$, a = 630.354(9) pm, c = 943.018(16) pm). To locate the hydrogen positions, neutron powder diffraction experiments on the deuterides were performed. Rietveld refinement (Figure 1 and Figure S1 in the Supporting Information) of the crystal structures confirmed the $LaMg_2D_7$ type and yielded precise structural parameters (Table 3 and Table S1 in the Supporting Information). For the corresponding investigations on $PrMg_2D_7$ and their evaluation see the Supporting Information.

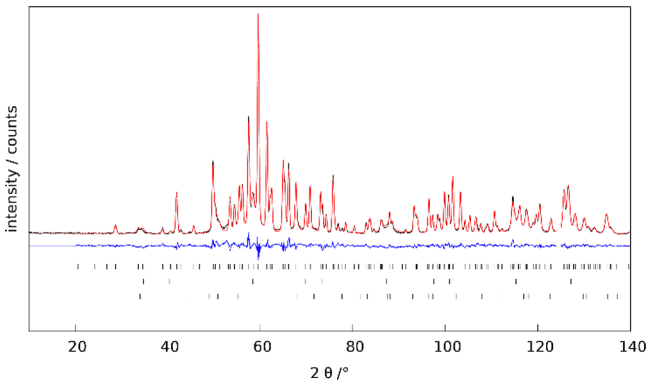

Figure 1. Rietveld refinement (black: measured; red: calculated; blue: difference diagram ($I_{obs} - I_{calc}$)) of the crystal structure of $NdMg_2D_7$ using neutron diffraction data (D20 at the Institut Laue-Langevin in Grenoble, France; λ = 186.78(3) pm); R_p = 2.87%, R_{wp} = 3.81%; Bragg positions from top to bottom: $NdMg_2D_7$ (73(1)%), NdD_2 (23(1)%), MgD_2 (3.8(1)%); data point at 2θ = 125° excluded because of detector failure.

Table 3. Crystal Structure of $NdMg_2D_7$[a]

atom	Wyckoff site	x	y	z	B_{iso}, 1×10^4 pm^2
Nd	4a	0.2699(3)	x	0	0.25(5)
Mg	8b	0.0287(4)	0.2629(5)	0.3514(3)	0.88(6)
D1	8b	0.0395(4)	0.0264(4)	0.1274(3)	1.86(5)
D2	8b	0.0824(4)	0.4339(4)	0.1815(2)	1.64(5)
D3	8b	0.3107(4)	0.1553(4)	0.2512(4)	2.07(6)
D4	4a	0.7547(5)	x	0	1.80(7)

[a] $P4_12_12$, a = 628.15(2) pm, c = 940.32(3) pm.

The crystal structures of the hydrides (deuterides) $NdMg_2H(D)_7$ are tetragonally distorted and hydrogen (deuterium)-filled variants of the parent cubic Laves phases $LnMg_2$ (Figure 2). Hydrogen (deuterium) atoms occupy four different crystallographic sites (Table 3). Two of them correspond to [Ln_2Mg_2] tetrahedral voids, one to an [Mg_4] tetrahedral void, and one exhibits a trigonal planar coordination (Figure 3).

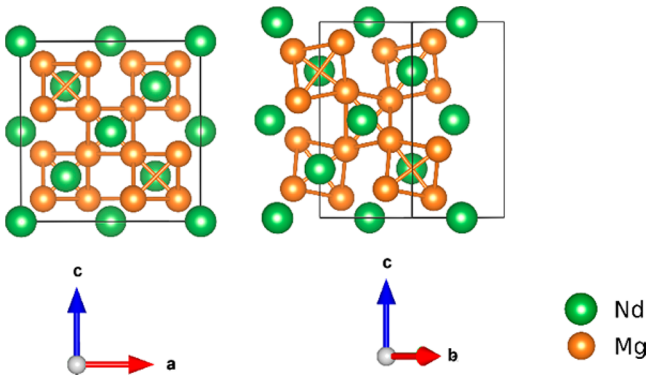

Figure 2. Crystal structures of $NdMg_2$ (left, view along [010]) and $NdMg_2D_7$ (right, view along [$\bar{1}$10], deuterium atoms omitted for clarity), emphasizing corner-sharing Mg_4 tetrahedra.

The mutual coordination spheres of neodymium and magnesium are similar to that in the parent cubic Laves phase. Neodymium atoms are coordinated 16-fold by a [La_4]

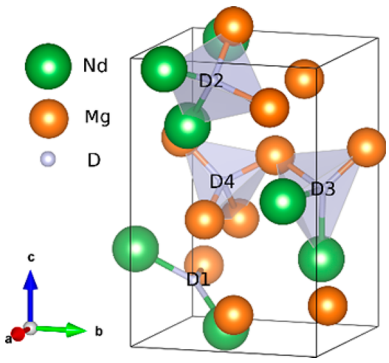

Figure 3. Crystal structure of $NdMg_2D_7$ with coordination polyhedra of the deuterium atoms.

DOI: 10.1021/acs.inorgchem.7b02319
Inorg. Chem. XXXX, XXX, XXX−XXX

tetrahedron, which is capped by 12 magnesium atoms. Magnesium atoms are icosahedrally coordinated by six magnesium and six neodymium atoms.

In the hydrides (deuterides), both coordination polyhedra are distorted with respect to the hydrogen-free parent cubic Laves phases $LnMg_2$ (Figure 4). In addition, lanthanide atoms

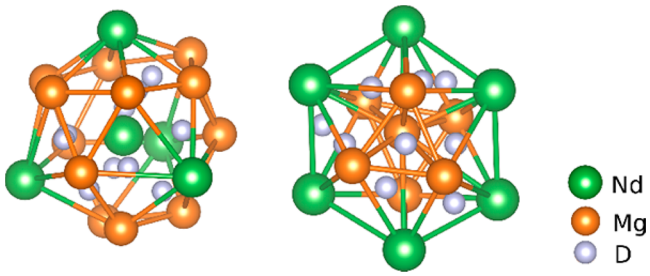

Figure 4. Coordination spheres of metal atoms in the crystal structure of $NdMg_2D_7$.

are coordinated by 12 hydrogen (deuterium) atoms, and magnesium is coordinated by seven hydrogen (deuterium) atoms. These metal−hydrogen (deuterium) polyhedra are strongly distorted and are related to an anti-cuboctahedron and a monocapped trigonal prism, respectively.

The structural similarities of the cubic Laves phases $LnMg_2$ and their hydrides (deuterides) $LnMg_2H(D)_7$ manifest themselves in crystallographic group−subgroup relationships. They are very useful tools for the analysis of ordering phenomena in intermetallic compounds.[38,39] The corresponding *Bärnighausen* tree (Figure 5) shows two possible ways to reduce the symmetry of the parent structure in the $MgCu_2$ type: (i) a *translationengleiche* transformation of index 3 (t3) to space group $I4_1/amd$ followed by a transition t2 and (ii) a transition t2 to space group $F4_132$ followed by a transformation t3 to space group $I4_122$. The final step in symmetry reduction is a *klassengleiche* transformation of index 2 to space group $P4_12_12$ (Figure 5). With the *Bärnighausen* formalism, the refined atomic positions of the heavy atoms of $LnMg_2(H)D_7$ may now be compared with the aristotype $MgCu_2$ of $LnMg_2$. Structural parameters do not differ much between the cubic Laves phases $LnMg_2$ and their hydrides (deuterides) phases $LnMg_2H(D)_7$. For example, the position of the Nd atom on the Wyckoff position 4*a* (*x*, *x*, 0 with $x = 0.2699(3)$) differs only slightly from the ideal value of 0.25 as transformed from the $MgCu_2$ type (Figure 5). The translational symmetry, however, shows substantial deviation from cubic with $\sqrt{2}*a/c = 0.945$ for $NdMg_2D_7$; that is, the *c* axis expands considerably more upon hydrogenation than the *a* axis. Because of the lanthanide contraction the lattice parameters of the hydrides decrease with atomic number of the lanthanide (Table 4). The interatomic distances follow this trend closely (Table 5).

The hydrides $LnMg_2H_7$ differ considerably from other Laves phase hydrides. They show the highest hydrogen content, which is achieved by distorting the Laves phase structure in a way as to allow hydrogen atoms to shift away from the tetrahedral voids. In contrast to most other Laves phase hydrides they exhibit an ordered hydrogen distribution at room temperature and semiconducting behavior; that is, the hydrogenation reaction is accompanied by a metal−semiconductor transition. The volume increments of hydrogen in $LnMg_2H_7$ compounds are calculated to range from to 6.2 (for Ln = Sm) to 6.7 cm^3/mol (for Ln = La). They are thus between the

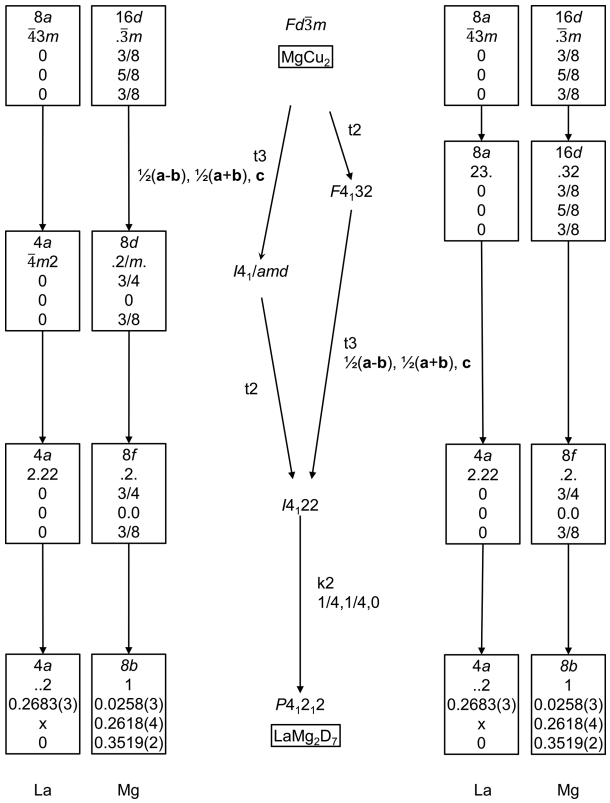

Figure 5. Crystallographic group−subgroup relationships (*Bärnighausen* tree[36,37]) showing the structural relation between the cubic Laves phases $LnMg_2$ (Ln = La, Ce, Pr, Nd, Sm; $MgCu_2$ type, C15) and their hydrides in the tetragonal $LaMg_2D_7$ type of structure. The evolution of the positional parameters is shown only for the Ln and Mg atoms. Zero (0) and fractional numbers (e.g., 1/2, 3/8) denote fixed, rational numbers (e.g., 0.0, 0.5, 0.375) free positional parameters.

values for LaH_2 and LaH_3 and suggest a considerable ionic contribution to chemical bonding.[40,41]

Hydrides $LnMg_2H_x$ of the Late Lanthanides (Ln = Eu, Gd, Tb). The hydrogenation of the hexagonal Laves phase $EuMg_2$ under a pressure of 12.0 MPa and a temperature of 353 K resulted in the formation of a new phase. The X-ray diffraction pattern resembles that of a hexagonal Laves phase with expanded unit cell. A closer inspection, however, especially of high-resolution synchrotron diffraction data, reveals reflection splitting (Figure 6). The diffraction pattern was indexed with an orthorhombic unit cell with $a = 664.9$ pm, $b = 1137.0$ pm, and $c = 1069.9$ pm. Systematic reflection absences suggested space group $P2_12_12_1$. A structure model was derived by group−subgroup relationships (Figure 7). The symmetry reduction to space group $P2_12_12_1$ was conducted in such a way as to properly describe the lattice parameters found by the indexing procedure. Rietveld refinement with starting parameters as derived for space group $P2_12_12_1$ (Figure 7) yielded a good correspondence between observed and calculated diffraction patterns (Figure 6). Trying the higher symmetric models clearly revealed the absence of *C*-centering.

Upon hydrogenation of $EuMg_2$ and formation of the hydride $EuMg_2H_x$, all lattice parameters increase, resulting in a volume increase of 11% (Table 6). This clearly indicates hydrogen incorporation. The volume increase, however, is somewhat smaller than for $LnMg_2H_7$ (Table 4), suggesting a lower hydrogen content. The crystal structure resembles a distorted

DOI: 10.1021/acs.inorgchem.7b02319
Inorg. Chem. XXXX, XXX, XXX−XXX

Table 4. Lattice Parameters and Unit-Cell Volumes of the Ternary Deuterides $LnMg_2D_7$ (Ln = La, Ce, Pr, Nd, Sm) and Relative Increase Δ with Respect to the Hydrogen-Free Laves Phases[a]

unit cell	$LaMg_2D_7$	$CeMg_2D_7$	$PrMg_2D_7$	$NdMg_2D_7$	$SmMg_2D_7$
a, pm	639.00(2)	635.01(3)	630.56(2)	628.15(2)	624.10(1)
c, pm	957.82(4)	949.57(2)	943.27(3)	940.32(3)	934.81(2)
V, 1×10^6 pm^3	391.10(3)	382.90(3)	375.05(2)	371.03(2)	364.11(1)
Δ*a*	3%	3%	3%	3%	2%
Δ*c*	9%	9%	9%	9%	8%
Δ*V*	15.8%	14.9%	14.3%	14.2%	13.8%

[a]Accounting for lattice parameter transformation, see Figure 5.

Table 5. Selected Interatomic Distances in the Crystal Structures of $LnMg_2D_7$[a]

atom pair	La	Ce	Pr	Nd	Sm
D1-Ln	246.9(4)	246.3(4)	242.0(7)	242.3(4)	240.5(8)
	240.9(4)	236.2(4)	234.1(7)	231.5(4)	231.6(8)
D1-Mg	192.1(4)	190.4(4)	192.4(6)	194.1(5)	185.3(9)
D2-Ln	246.6(4)	243.7(4)	241.1(8)	239.4(4)	242.4(9)
	238.8(3)	236.0(3)	232.4(6)	231.5(3)	227.6(7)
D2-Mg	213.1(4)	217.9(4)	216.4(6)	215.6(4)	219.7(9)
	199.1(3)	199.0(4)	195.8(6)	195.5(4)	194.8(9)
D3-Ln	255.4(3)	252.9(3)	251.3(8)	248.3(4)	246.8(8)
	255.0(3)	250.7(4)	259.4(6)	247.3(4)	246.2(8)
D3-Mg	211.6(3)	211.8(3)	211.1(6)	211.7(5)	207(1)
	203.2(4)	201.2(4)	201.8(6)	201.5(5)	205(1)
D4-Mg	206.2(3)	202.7(3)	202.4(6)	202.2(4)	198.2(8)
	198.2(3)	198.0(3)	196.9(6)	195.3(4)	196.9(9)

[a]In picometers. Ln = La, Ce,[20] Pr, Nd (this work), and Sm[21].

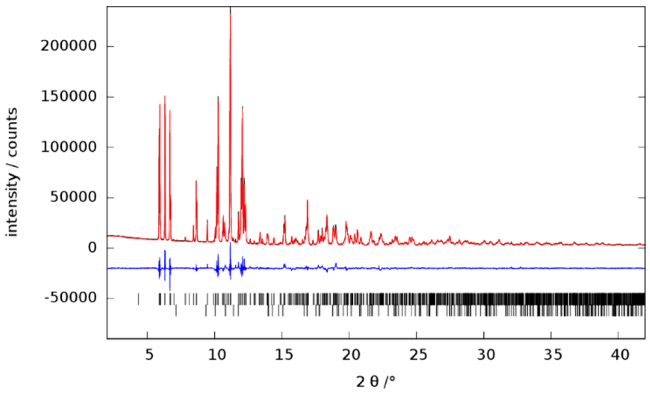

Figure 6. Rietveld refinement (black: measured; red: calculated; blue: difference diagram ($I_{obs} - I_{calc}$)) of the crystal structure of $EuMg_2H_x$ using synchrotron diffraction data (powder diffraction beamline, Australian Synchrotron, Melbourne, Australia, λ = 58.9074 pm); R_p = 4.85%, R_{wp} = 6.64%; Bragg positions from top to bottom: $EuMg_2H_x$ (98.24(5)%), EuH_2 (1.76(5)%).

hexagonal Laves phase. In contrast to the parent hexagonal Laves phase the faces shared by Mg_4 tetrahedra are slightly inclined toward each other in the hydride (Figure 8). Because of the symmetry reduction, there are two crystallographically different europium atoms and four crystallographically different magnesium atoms in the crystal structure of the hydride. The coordination of the atoms is similar to the atoms in the cubic Laves phases. Both europium atoms are 16-fold coordinated and located within distorted Frank–Kasper polyhedra. All four magnesium atoms are coordinated by a distorted icosahedron. Interestingly, so far there are only a few hydrides based on hexagonal Laves phases known, for example, $ZrCr_2H_{3.8}$.[42]

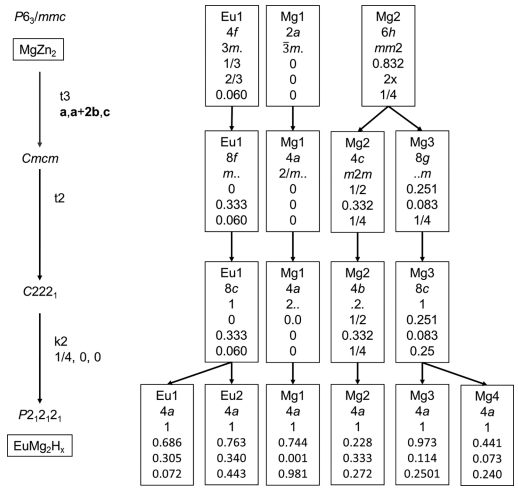

Figure 7. Crystallographic group–subgroup relationships (*Bärnighausen* tree[38,39]) showing the structural relation (for the metal positions) between the hexagonal Laves phase $EuMg_2$ ($MgZn_2$ type, C14) and its hydride $EuMg_2H_x$. Zero (0) and fractional numbers (e.g., 1/2, 3/8) denote fixed, rational numbers (e.g., 0.0, 0.5, 0.375) free positional parameters.

Table 6. Lattice Parameters and Unit Cell Volumes of the Laves Phase $EuMg_2$[a] and Its Hydride $EuMg_2H_x$

compound	*a*, pm	b_{ortho}, pm	*c*, pm	*V*, 1×10^6 pm^3
$EuMg_2$	638.77(9)	1106.38	1032.23(19)	729.5(3)
$EuMg_2H_x$	664.887(4)	1136.993(7)	1069.887(7)	808.80(1)

[a]Orthogonalized, that is, $b_{ortho} = 2 \times \cos 30° \, a_{hex}$.

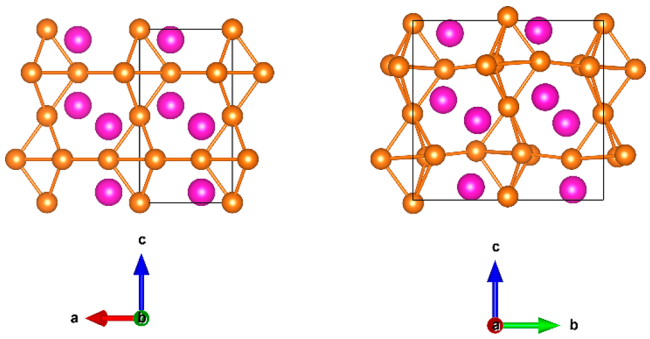

Figure 8. Comparison of the crystal structures of $EuMg_2$ (left) and $EuMg_2H_x$ (right).

The compound $EuMg_2H_x$ was the first example in the system Ln–Mg–H, which has a structural relationship to the crystal structure of the parent $LnMg_2$ compounds crystallizing in the $MgZn_2$ type. So it was obvious to investigate the hydrogenation

DOI: 10.1021/acs.inorgchem.7b02319
Inorg. Chem. XXXX, XXX, XXX–XXX

Table 7. Crystal Structure of $EuMg_2H_x$[a]

atom	Wyckoff site	x	y	z	B_{iso}, 1×10^4 pm^2
Eu1	4a	0.68629(11)	0.30514(7)	0.07208(9)	1.39(2)
Eu2	4a	0.76379(12)	0.34032(7)	0.44317(8)	B_{iso}(Eu1)
Mg1	4a	0.7441(8)	0.0019(5)	0.9813(5)	1.55(6)
Mg2	4a	0.2282(9)	0.3332(5)	0.2721(6)	B_{iso}(Mg1)
Mg3	4a	0.9735(8)	0.1149(5)	0.2501(7)	B_{iso}(Mg1)
Mg4	4a	0.4413(8)	0.0738(5)	0.2401(7)	B_{iso}(Mg1)

[a] $P2_12_12_1$, a = 664.887(4) pm, b = 1136.993(7) pm, c = 1069.887(7) pm.

behavior of hexagonal Laves phases $LnMg_2$ of the heavier lanthanides. The compounds $GdMg_2$ and $TbMg_2$ form new phases under hydrogen pressure. The X-ray powder diffraction pattern of $GdMg_2H_x$ was indexed with an orthorhombic cell with a = 1282.7 pm, b = 572.5 pm, and c = 881.7 pm. The lattice parameter ratios are similar to the tetragonal $LnMg_2D_7$, but with a doubled a lattice parameter. The X-ray powder diffraction pattern of $TbMg_2H_x$ was indexed with an orthorhombic cell with a = 617.8 pm, b = 1045.8 pm, and c = 997.1 pm. The lattice parameter ratios are very similar to $EuMg_2H_x$; however, a structure refinement using this structure model was not successful. For neither of the phases $GdMg_2H_x$ and $TbMg_2H_x$ a structure model was found, but Pawley fits were performed yielding refined lattice parameters (Figures S2 and S3 in Supporting Information). The increase in volume is 3.53% for $GdMg_2H_x$ and 5.02% for $TbMg_2H_x$. Compared to $EuMg_2H_x$ (Table 7) and $LnMg_2H_7$ the volume increase upon hydrogenation is lower and suggests a lower hydrogen content. An in situ experiment was performed for $GdMg_2$ under a hydrogen gas pressure of 10.0 MPa. In situ investigations of chemical reactions are very useful to reveal reaction pathways and discover possible intermediates.[43−46] Unfortunately, $GdMg_2$ did not form the ternary hydride under these conditions, but first GdH_2 at 463 K and then GdH_3 at 543 K formed (Figure S4 in Supporting Information).

Thermal Stability and Reactivity toward Air. The thermal stabilities of the Laves phase hydrides $LnMg_2H_7$ were investigated by thermal analysis under 0.1 MPa hydrogen gas pressure up to 723 K (Figure 9). The onset of the signals associated with decomposition of $LnMg_2H_7$ are at 639 K ($SmMg_2H_7$), 672 K ($NdMg_2H_7$), 684 K ($PrMg_2H_7$), 684 K ($CeMg_2H_7$), and 695 K ($LaMg_2H_7$). Using helium instead of hydrogen atmosphere did not change the decomposition temperatures significantly. The decomposition temperature decreases with increasing atomic number of the lanthanides, indicating a reduced thermal stability of $LnMg_2H_7$ for the heavier lanthanides. The decomposition reaction is irreversible by and large as proven by the weak exothermic signal upon cooling and the reaction products found by X-ray powder diffraction after the experiment, being LnH_2 and elemental Mg. Despite their mainly ionic nature, the hydrides $LnMg_2H_7$ are stable in air for several days. This is quite remarkable and very uncommon for ionic hydrides.

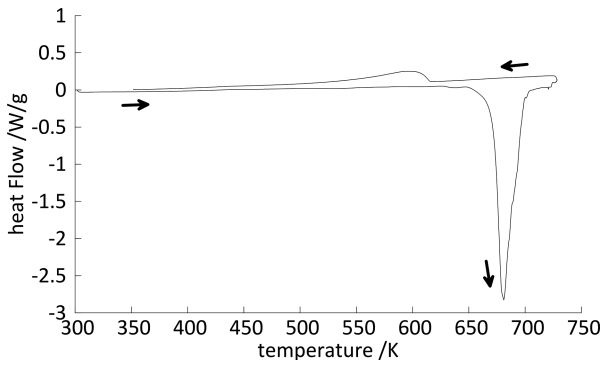

Figure 9. In situ thermal analysis (DSC, exothermic signal up, endothermic signals down) of the decomposition of $NdMg_2H_7$ under 0.1 MPa hydrogen atmosphere.

The Laves phase $NdMg_2$ was substituted with 5 atom % of samarium or terbium. Powdered samples of $Nd_{0.95}Sm_{0.05}Mg_2$ and $Nd_{0.95}Tb_{0.05}Mg_2$ were hydrogenated under the same conditions as for the unsubstituted compounds. The lattice parameters as refined by the Rietveld method were smaller for substituted than for the unsubstituted $NdMg_2$ (Table 8), which indicated a successful substitution. Excitation with UV light (240 and 360 nm) did not yield emission visible for the unaided human eye.

Table 8. Lattice Parameters[a] of Pure and Substituted $Nd_{0.95}Sm_{0.05}Mg_2H_7$ and $Nd_{0.95}Tb_{0.05}Mg_2H_7$

compound	$NdMg_2H_7$	$Nd_{0.95}Sm_{0.05}Mg_2H_7$	$Nd_{0.95}Tb_{0.05}Mg_2H_7$
a, pm	630.134(9)	629.594(8)	629.352(8)
c, pm	942.695(16)	942.307(15)	942.063(16)

[a] In picometers.

Magnetic Properties of $CeMg_2H_7$ and $NdMg_2H_7$. For both compounds the temperature dependence of the magnetic susceptibility (χ) was measured at 10 kOe (Figures 10 and 11, top). The samples show paramagnetism over the whole investigated temperature range. The measured susceptibility was corrected for diamagnetic contributions (-8.3×10^{-4} emu mol^{-1} for $CeMg_2H_7$ and -6.3×10^{-4} emu mol^{-1} for $NdMg_2H_7$) caused, for example, by the capsule and traces of impurities. These contributions were obtained by fitting the magnetic data in the temperature range from 100 to 300 K using the modified Curie−Weiss law. From the inverse susceptibility data (χ^{-1}) the effective magnetic moment was determined. For $CeMg_2H_7$ μ_{eff} = 2.49(1) μ_B was calculated, and for $NdMg_2H_7$ μ_{eff} = 3.62(1) μ_B was calculated; these values are in good agreement with the calculated magnetic moments of the free trivalent rare-earth cations ($\mu_{calc}(Ce^{3+})$ = 2.54 μ_B; $\mu_{calc}(Nd^{3+})$ = 3.62 μ_B). Both measurements exhibit pronounced curvatures at low temperatures, which can be attributed to crystal field splitting of the magnetic ground states, a phenomenon often observed in rare-earth compounds.[47] Ternary and quaternary cerium hydrides have been summarized recently in two review articles.[48,49]

In addition, low-field measurements with a flux density of 100 Oe were performed in a zero-field-cooled and field-cooled modes (ZFC/FC). For $NdMg_2H_7$ (Figures 10 and 11, middle) again only paramagnetism was observed. $CeMg_2H_7$ exhibits a

DOI: 10.1021/acs.inorgchem.7b02319
Inorg. Chem. XXXX, XXX, XXX−XXX

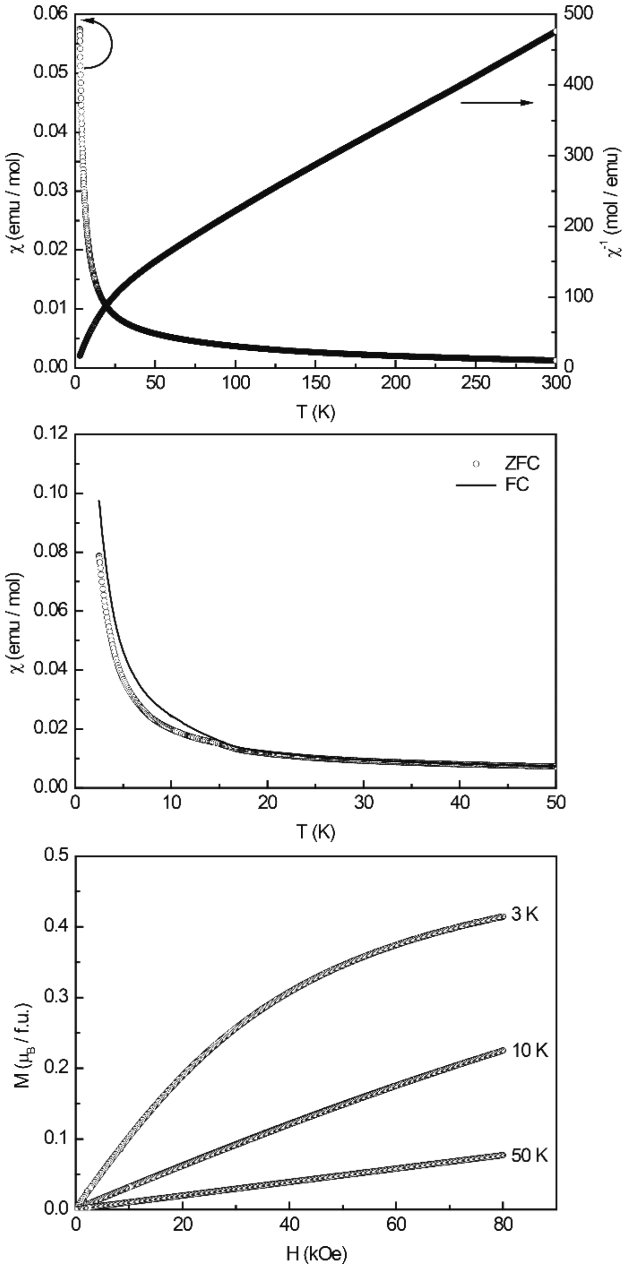

Figure 10. Magnetic properties of $CeMg_2H_7$: (top) temperature dependence of the magnetic susceptibility (χ and χ^{-1} data) measured at 10 kOe; (middle) ZFC/FC measurements at 100 Oe; (bottom) magnetization isotherms at 3, 10, and 50 K.

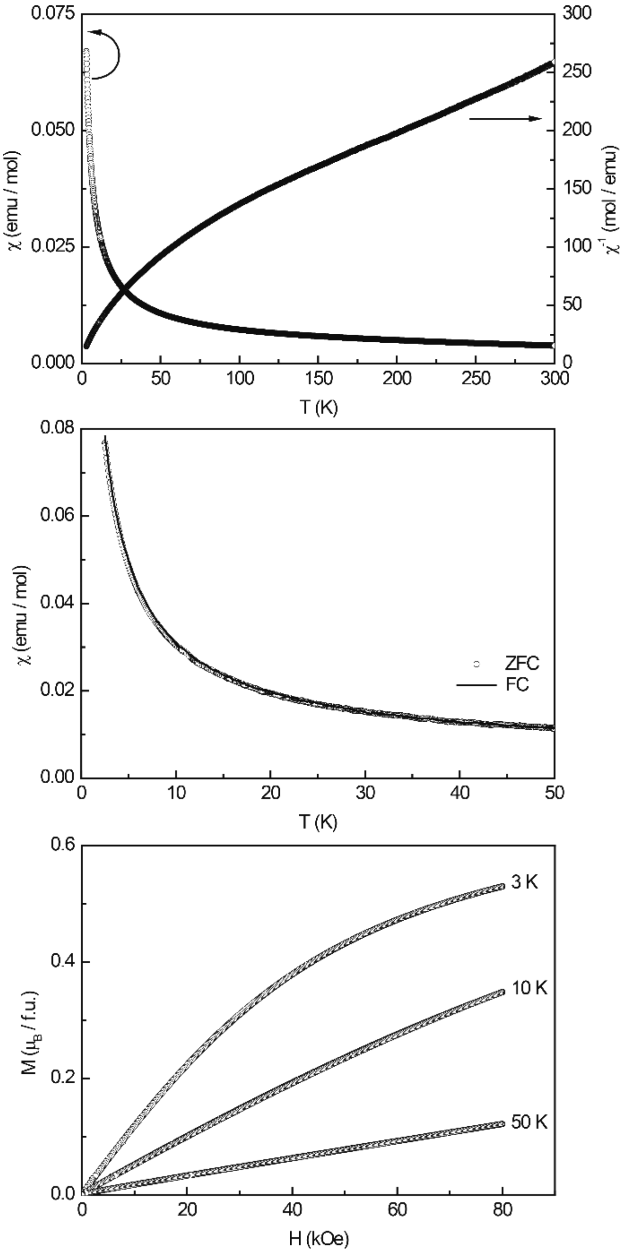

Figure 11. Magnetic properties of $NdMg_2H_7$: (top) temperature dependence of the magnetic susceptibility (χ and χ^{-1} data) measured at 10 kOe; (middle) ZFC/FC measurements at 100 Oe; (bottom) magnetization isotherms at 3, 10, and 50 K.

slight anomaly at T = 15 K (Figures 10 and 11, middle). Because of the rise in the susceptibility and the disappearance in the high-field experiments, this feature must be caused by traces of a ferromagnetic impurity. Ferromagnetic substances, however, exhibit susceptibilities that are several orders of magnitude higher than the ones of paramagnetic compounds. Possible impurities that could form and are known from literature are, for example, binary cerium hydrides, along with CeMg, $CeMg_2$, or $CeMg_3$. While the latter one and CeMg order anti-ferromagnetically at T_N = 2.6 K[50] and T_N = 20 K,[51,52] $CeMg_2$ orders ferromagnetically at T_C = 3.6 K.[53] For binary cerium hydrides CeH_2 and the series of CeH_{2+x} ($0 \leq x \leq 0.65$) have been investigated. Susceptibility measurements indicate that CeH_2 orders anti-ferromagnetically at $T_N \approx 7$ K;[54] for CeH_{2+x} ($0 \leq x \leq 0.65$) resistivity measurements were conducted. Samples with x = 0.4, 0.6, and 0.65 all exhibit ordering temperatures of T < 5 K.[55]

Finally magnetization isotherms at 3, 10, and 50 K were recorded. The 10 and 50 K isotherms exhibit linear field dependencies, consistent with paramagnetic behavior. The 3 K isotherms both exhibit slight curvatures with tendencies for saturation at high fields. For $CeMg_2H_7$ (Figure 10, bottom) a saturation magnetization of μ_{sat} = 0.41(2) μ_B per Ce atom at 3 K and 80 kOe can be found, for $NdMg_2H_7$ (Figure 10, middle) μ_{sat} = 0.53(2) μ_B per Nd atom at 3 K and 80 kOe is observed. Both values are significantly lower than the expected saturation magnetization of 2.14 μ_B (Ce^{3+}) and 3.27 μ_B (Nd^{3+}) according to $g_J \times J$.[56]

DOI: 10.1021/acs.inorgchem.7b02319
Inorg. Chem. XXXX, XXX, XXX−XXX

4. CONCLUSION

The class of Laves phase-based hydrides $LnMg_2H_7$ was extended by two members, that is, for Ln = Pr, Nd. Their crystal structures as derived by neutron powder diffraction on the deuterides are very similar to those known for Ln = La, Ce, Sm. The structural relationship to the cubic $MgCu_2$ type of the parent Laves phases can be shown by crystallographic group−subgroup relationships (*Bärnighausen* tree). Hydrides with the $LnMg_2D_7$ structure type are only formed by the earlier lanthanides, which exhibit the $MgCu_2$ structure type in Laves phases $LnMg_2$. These ternary hydrides form only at high hydrogen gas pressures and low-to-moderate temperatures. Lower hydrogen gas pressure and higher temperature favor the formation of binary hydrides instead. New hydrides were also found by hydrogenation of the hexagonal Laves phases $LnMg_2$ (Ln = Eu, Gd, Tb). $EuMg_2H_x$ shows an orthorhombic structure, which is a distortion variant of the parent hexagonal Laves phase type of $MgZn_2$. The lattice parameters suggest the same to be the case for $GdMg_2H_x$ and $TbMg_2H_x$. Despite the high hydrogen capacity the Laves phases $LnMg_2$ are not well-suited for hydrogen storage. The formation condition with hydrogen gas pressures of 9.0 MPa and higher are not practical, and the decomposition temperatures of the hydrides above 660 K are rather high. Magnetic measurements show that the ternary hydrides $CeMg_2H_7$ and $NdMg_2H_7$ exhibit no long-range magnetic ordering and remain paramagnetic down to 2.5 K and that the rare-earth atoms are in the trivalent oxidation state.

■ ASSOCIATED CONTENT

Supporting Information

The Supporting Information is available free of charge on the ACS Publications website at DOI: 10.1021/acs.inorgchem.7b02319.

Rietveld plot and refined structure data for $PrMg_2D_7$, Pawley refinements for $GdMg_2H_x$ and $TbMg_2H_x$, in situ powder diffraction of the hydrogenation of $GdMg_2$ (PDF)

Further details of the crystal structure investigations may be obtained from FIZ Karlsruhe, 76344 Eggenstein-Leopoldshafen, Germany (fax: (+49)7247−808−666; e-mail: crysdata@fiz-karlsruhe.de, on quoting the deposition numbers CSD-433615 ($PrMg_2D_7$), CSD-433616 ($NdMg_2D_7$), and CSD-433617 ($EuMg_2H_x$).

■ AUTHOR INFORMATION

Corresponding Author

*E-mail: holger.kohlmann@uni-leipzig.de.

ORCID

Oliver Janka: 0000-0002-9480-3888

Holger Kohlmann: 0000-0002-8873-525X

Author Contributions

The manuscript was written through contributions of all authors.

Funding

This work was funded by the Deutsche Forschungsgemeinschaft (DFG, Ko1803/4−1).

Notes

The authors declare no competing financial interest.

■ ACKNOWLEDGMENTS

The Institut Laue-Langevin, Grenoble, France, and the powder diffraction beamline at the Australian Synchrotron, Australia are acknowledged for providing beam time.

■ DEDICATION

Dedicated to Prof. Dr. Thomas Schleid on the occasion of his 60th birthday.

■ REFERENCES

(1) Reckeweg, O.; Di Salvo, F. J.; Wolf, S.; Schleid, T. Two Ternary Mixed-Anion Chlorides with Divalent Europium: Eu_2H_3Cl and $Eu_7F_{12}Cl_2$. T. *Z. Anorg. Allg. Chem.* **2014**, *640*, 1254−1259.

(2) Kohlmann, H.; Bertheville, B.; Hansen, T. C.; Yvon, K. High pressure synthesis of novel europium magnesium hydrides. *J. Alloys Compd.* **2001**, *322*, 59−68.

(3) Folchnandt, M.; Schleid, T. $Cs_3Y_7Se_{12}$: A New Ternary Compound in the Cs_2Se−Y_2Se_3 System. *Z. Kristallogr. Suppl.* **1996**, *11*, 79.

(4) Simon, A. Oxidation durch Wasserstoff in der Chemie und Physik der Seltenerdmetalle. *Angew. Chem.* **2012**, *124*, 4354−4361.

(5) Yartys, V. A.; Vajeeston, P.; Riabov, A. B.; Ravindran, P.; Denys, R. V.; Maehlen, J. P.; Delaplane, R. G.; Fjellvåg, H. Crystal chemistry and metal-hydrogen bonding in anisotropic and interstitial hydrides of intermetallics of rare earth (R) and transition metals (T), RT_3 and R_2T_7. *Z. Kristallogr.* **2008**, *223*, 674−689.

(6) Yvon, K.; Rapin, J.-P.; Penin, N.; Ma, Z.; Chou, M. Y. $LaMg_2PdH_7$, a new complex metal hydride containing tetrahedral $[PdH_4]^{4-}$ anions. *J. Alloys Compd.* **2007**, *446*−*447*, 34−38.

(7) Kohlmann, H.; Moyer, R. O., Jr.; Hansen, T.; Yvon, K. X-ray and neutron powder diffraction study of the order-disorder transition in Eu_2IrH_5 and the mixed crystal compounds $Eu_{2-x}A_xIrH_5$ (A = Ca, Sr; x = 1.0, 1.5). *J. Solid State Chem.* **2003**, *174*, 35−43.

(8) Fruchart, D.; Rouault, A.; Shoemaker, C. B.; Shoemaker, D. P. Neutron Diffraction Studies of the Cubic $ZrCr_2D_x$ and $ZrV_2D_x(H_x)$. *Phys. stat. sol.* **1980**, *57*, 119−122.

(9) Johnson, J. R.; Reilly, J. J. Reaction of hydrogen with the low-temperature form (C15) of titanium-chromium ($TiCr_2$). *Inorg. Chem.* **1978**, *17*, 3103−3108.

(10) Shaltiel, D. Hydride Properties of AB_2 Laves Phase Compounds. *J. Less-Common Met.* **1978**, *62*, 407−41.

(11) Shoemaker, D. P.; Shoemaker, C. B. Concerning Atomic Sites and Capacities for Hydrogen Absorption in the AB_2 Friauf-Laves Phases. *J. Less-Common Met.* **1979**, *68*, 43−58.

(12) Irodova, A. V.; Somenkov, V. A.; Shil'stein, S. Sh. Coordination of hydrogen in metals and intermetallic compounds. *Sov. Phys. Solid State* **1983**, *25*, 1845−1847.

(13) Yvon, K.; Fischer, P. Crystal and Magnetic Structures of Ternary Metal Hydrides: A Comprehensive Review. In: *Hydrogen in Intermetallic Compounds I;* Schlapbach, L., Ed.; Topics in Applied Physics; Springer: Berlin, Germany, **1988**; Vol. *63*, pp 87−138.10.1007/3540183337_11

(14) Kohlmann, H.; Fauth, F.; Yvon, K. Hydrogen order in monoclinic $ZrCr_2H_{3.8}$. *J. Alloys Compd.* **1999**, *285*, 204−211.

(15) Kohlmann, H.; Fauth, F.; Fischer, P.; Skripov, A. V.; Yvon, K.; et al. Low-temperature deuterium ordering in the cubic Laves phase derivative α-$ZrCr_2D_{0.66}$. *J. Alloys Compd.* **2001**, *327*, L4−L9.

(16) Kohlmann, H. Comment on "Structural and Electronic Properties of the Hydrogenated $ZrCr_2$ Laves Phases". *J. Phys. Chem. C* **2010**, *114*, 13153.

(17) Filipek, S. M.; Paul-Boncour, V.; Kuriyama, N.; Takeichi, N.; Tanaka, H.; Liu, R. S.; Wierzbicki, R.; Sato, R.; Kuo, H. T. Hydrides of Laves phases intermetallic compounds synthesized under high hydrogen pressure. *Solid State Ionics* **2010**, *181*, 306−310.

(18) Paul-Boncour, V.; Filipek, S. M.; Sato, R.; Wierzbicki, E.; André, G.; Porcher, F.; Reissner, M.; Wiesinger, G. Structural and magnetic properties of $RMn_{2-x}Fe_xD_6$ compounds (R = Y, Er; x = ≤ 0.2)

DOI: 10.1021/acs.inorgchem.7b02319
Inorg. Chem. XXXX, XXX, XXX−XXX

synthesized under high deuterium pressure. *J. Solid State Chem.* **2011**, *184*, 463−469.
(19) Gschneidner, A. K., Jr.; Pecharsky, V. K. Binary rare earth Laves phases - an overview. *Z. Kristallogr.* **2006**, *221*, 375−381.
(20) Gingl, F.; Yvon, K.; Vogt, T.; Hewat, A. Synthesis and crystal structure of tetragonal $LnMg_2H_7$ (Ln = La, Ce), two Laves phase hydride derivatives having ordered hydrogen distribution. *J. Alloys Compd.* **1997**, *253*−*254*, 313−317.
(21) Kohlmann, H.; Werner, F.; Yvon, K.; Hilscher, G.; Reissner, M.; Cuello, G. J. Neutron Powder Diffraction with ^{nat}Sm: Crystal Structures and Magnetism of a Binary Samarium Deuteride and a Ternary Samarium Magnesium Deuteride. *Chem. - Eur. J.* **2007**, *13*, 4178−4186.
(22) Kohlmann, H.; Gingl, F.; Hansen, T.; Yvon, K. The First Determination of Eu-H Distances by Neutron Diffraction on the Novel Hydrides $EuMg_2H_6$ and $EuMgH_4$. *Angew. Chem., Int. Ed.* **1999**, *38*, 1856−2070.
(23) Kohlmann, H.; Yvon, K.; Wang, Y. Synthesis, crystal structure and magnetism of the mixed metal hydrides $Eu_{1-x}Sr_xMg_2H_6$ ($0 \leq x \leq 0.6$). *J. Alloys Compd.* **2005**, *393*, 11−15.
(24) Blaschkowski, B.; Schleid, B. Einkristalle von $LiEuH_3$ und $LiBaH_3$ mit "inverser" Perowskit-Struktur. *Z. Anorg. Allg. Chem.* **2006**, *632*, 2149.
(25) Yvon, K.; Kohlmann, H.; Bertheville, B. Europium-hydrogen bond distances in saline metal hydrides by neutron diffraction. *Chimia* **2001**, *55*, 505−509.
(26) Kohlmann, H. Structural relationships in complex hydrides of the late transition metals. *Z. Kristallogr.* **2009**, *224*, 454−460.
(27) Gschneidner, K. A. *Rare Earth Alloys;* Van Nostrand Co. Inc.: New York, 1961.
(28) Kohlmann, H. Hydrogenation of palladium rich compounds of aluminium, gallium and indium. *J. Solid State Chem.* **2010**, *183*, 367−372.
(29) Auer, H.; Kohlmann, H. In situ Investigations on the Formation and Decomposition of $KSiH_3$ and $CsSiH_3$. *Z. Anorg. Allg. Chem.* **2017**, *643*, 945−951.
(30) Rietveld, H. M. Line profiles of neutron powder-diffraction peaks for structure refinement. *Acta Crystallogr.* **1967**, *22*, 151−152.
(31) Rietveld, H. M. A Profile Refinement Method for Nuclear and Magnetic Structures. *J. Appl. Crystallogr.* **1969**, *2*, 65−71.
(32) Bruker AXS, TOPAS version 5, https://www.bruker.com.
(33) Rodrıguez-Carvajal, J. Recent advances in magnetic structure determination neutron powder diffraction. *Phys. B* **1993**, *192*, 55−69.
(34) Rodrıguez-Carvajal, J. *FullProf.2k,* Version 5.30-Mar2012-ILL JRC; Institute Laue-Langevin, 2012.
(35) VESTA-Visualisation for Electronic and Structural Analysis, version 3.3.1
(36) Bärnighausen, H. Group-Subgroup Relations Between Space Groups: A Useful Tool in Crystal Chemistry. *MATCH* **1980**, *9*, 139−175.
(37) Müller, U. Kristallographische Gruppe-Untergruppe-Beziehungen und ihre Anwendung in der Kristallchemie. *Z. Anorg. Allg. Chem.* **2004**, *630*, 1519−1537.
(38) Pöttgen, R. Coloring, Distortions, and Puckering in Selected Intermetallic Structures from the Perspective of Group-Subgroup Relations. *Z. Anorg. Allg. Chem.* **2014**, *640*, 869−891.
(39) Kohlmann, H.; Ritter, C. Reaction Pathways in the Formation of Intermetallic $InPd_3$ Polymorphs. *Z. Anorg. Allg. Chem.* **2009**, *635*, 1573−1579.
(40) Bronger, W. Die Raumchemie des Wasserstoffs in Metallhydriden im Vergleich mit entsprechenden Fluoriden und Chloriden. *Z. Anorg. Allg. Chem.* **1996**, *622*, 9−16.
(41) Bronger, W.; Kniep, R.; Kohout, M. Zur Raumchemie des Wasserstoffs in binären und ternären Metallhydriden. *Z. Anorg. Allg. Chem.* **2005**, *631*, 265−271.
(42) Kohlmann, H.; Yvon, K. Revision of the low-temperature structures of rhombohedral $ZrCr_2D_x$ ($x \sim 3.8$), and monoclinic ZrV_2D_x ($1.1 < x < 2.3$) and HfV_2D_x ($x \sim 1.9$). *J. Alloys Compd.* **2000**, *309*, 123−127.
(43) Widenmeyer, M.; Niewa, R.; Hansen, T. C.; Kohlmann, H. *In situ* Neutron Diffraction as a Probe on Formation and Decomposition of Nitrides and Hydrides: A Case Study. *Z. Anorg. Allg. Chem.* **2013**, *639*, 285−295.
(44) Møller, K. T.; Hansen, B. R. S.; Dippel, A.-C.; Jørgensen, J.-E.; Jensen, T. R. Characterization of Gas-Solid Reactions using In Situ Powder X-ray Diffraction. *Z. Anorg. Allg. Chem.* **2014**, *640*, 3029−3043.
(45) Hansen, T. C.; Kohlmann, H. Chemical Reactions followed by *in situ* Neutron Powder Diffraction. *Z. Anorg. Allg. Chem.* **2014**, *640*, 3044−3063.
(46) Auer, H.; Wallacher, D.; Hansen, T. C.; Kohlmann, H. In Situ Hydrogenation of the Zintl Phase SrGe. *Inorg. Chem.* **2017**, *56*, 1072−1079.
(47) Szytuła, A.; Leciejewicz, J. *Handbook of Crystal Structures and Magnetic Properties of Rare Earth Intermetallics;* CRC Press: Boca Raton, FL, 1994.
(48) Janka, O.; Niehaus, O.; Pöttgen, R.; Chevalier, B. Cerium intermetallics with TiNiSi-type structure. *Z. Naturforsch., B: J. Chem. Sci.* **2016**, *71*, 737−764.
(49) Pöttgen, R.; Janka, O.; Chevalier, B. Cerium intermetallics CeTX − review III. *Z. Naturforsch., B: J. Chem. Sci.* **2016**, *71*, 165−191.
(50) Das, P. K.; Kumar, N.; Kulkarni, R.; Thamizhavel, A. Magnetism in RMg_3 (R = La, Ce and Nd) Single Crystals. *J. Phys.: Conf. Ser.* **2012**, *391*, 012009.
(51) Schmitt, D.; Morin, P.; Pierre, J. Magnetic structure and crystal field in cerium compounds with CsCl-type structureOriginal Research Article. *J. Magn. Magn. Mater.* **1978**, *8*, 249−256.
(52) Aléonard, R.; Morin, P.; Pierre, J.; Schmitt, D. Magnetic properties of RMg compounds. *Physica B+C* **1977**, *86*−*88*, 95−96.
(53) Buschow, K. H. J.; Sherwood, R. C.; Hsu, F. S. L.; Knorr, K. Magnetic properties of rare-earth magnesium compounds of the type RMg_2. *J. Appl. Phys.* **1978**, *49*, 1510−1512.
(54) Burger, J. P.; Daou, J. N.; Vajda, P. Correlations between magnetism, electrical conductivity and structural ordering in rare earth hydrides REH_{2+x} Origin. *J. Magn. Magn. Mater.* **1990**, *90*−*91*, 110−114.
(55) Burger, J. P.; Vajda, P.; Daou, J. N. Study of structural ordering, kondo effects and magnetism in CeH_{2+x}, with $0 \leqslant x \leqslant 0.65$, through electrical resistivity measurements. *J. Phys. Chem. Solids* **1991**, *52*, 779−786.
(56) Lueken, H. *Magnetochemie;* B. G. Teubner, Stuttgart, Germany, 1999.

DOI: 10.1021/acs.inorgchem.7b02319
Inorg. Chem. XXXX, XXX, XXX−XXX